

# Shrinking core discharge model for the negative electrode of a lead-acid battery

B. Vijayasekaran, C. Ahmed Basha\*

*Central Electrochemical Research Institute, Karaikudi 630006, India*

Received 17 August 2005; received in revised form 29 September 2005; accepted 3 October 2005

Available online 15 November 2005

## Abstract

This article presents a shrinking core model for the discharge of porous lead particle at the negative electrode of a lead-acid battery by considering the reaction in a separate particle of the solid matrix. The model relates the shrinking unreacted lead core with the maximum amount of active material that can be reacted before termination of the discharge process due to poorly soluble low-conducting product. The developed model equations also incorporate the effect of double-layer capacitance and a dissolution–precipitation mechanism on the discharge process. The expressions for evaluating concentration and potential distributions as functions of time and distance are presented in three different models of a porous lead particle. For the simple case, equations are solved to achieve analytical expressions and where the coupled potential and concentration gradients with dissolution–precipitation mechanism are taken into account; the numerical method of lines is utilized to study the discharge behavior. The simulation outcomes are in good agreement when compared with the experimental data for discharge.

© 2005 Elsevier B.V. All rights reserved.

*Keywords:* Lead-acid battery; Negative electrode; Discharge; Unreacted-core shrinking; Electrode kinetics; Solid-state reaction

## 1. Introduction

Various idealized mathematical models have been proposed to explain the operation of porous lead electrode because of its great importance as the negative electrode in the lead-acid battery. The ultimate aim of such studies is the formulation of a model which can predict the performance of practical electrodes. It is possible with such a model to optimize the design of new cells, particularly cells for high-energy density or cells with a new configurations. In spite of the numerous investigations, that the porous lead electrode has been subjected to, there is still a need for more knowledge on the basis of explanations and predictions of the electrode behavior. Due to the extreme complexity of the interacting effects of electrochemical kinetics, structural changes and mass-transfer processes, it may not be possible to find one single model that adequately describes its behavior. In fact, the research on lead-acid batteries will grow for several more decades to come. The purpose of the present

study is to advance the art of modeling the porous lead electrode by combining a detailed fundamental model of a porous electrode with the concept of unreacted-core shrinking.

A number of detailed fundamental models for lead-acid batteries have been reported in the literature [1–17], and no attempt has been made to provide an exhaustive review. These models are typically one-dimensional, and include a detailed description of the physical, chemical and electrical processes that take place in the battery. Efforts in recent years have focused on modeling the behavior of recombinant cells, which have become increasingly important in commercial applications [18–20]. One can see that some models are based on the search for analytical solutions of the diffusion equation combined with an electrical circuit. These models can give much insight into a system, which is one of the primary objectives of modeling. The reason for this is that analytical solutions are continuous in the independent variables, and show explicitly how the parameters of the system are involved. More recent models [21–24] heavily rely on the solution of similar equation sets by means of digital simulation. The latter permits us to study a large range of parameters involved. The disadvantage, however, is that the results have to be accepted more or less blindly, while their contribution to a better understanding of the phenomena is minimal.

\* Corresponding author. Tel.: +91 4565 227555; fax: +91 4565 227779.

*E-mail addresses:* vijayasekaranb@yahoo.com (B. Vijayasekaran), basha@cecri.res.in (C.A. Basha).

Also most of these mathematical models are based on a macroscopic approach or employ continuum models. This involves numerical solution of model equations describing discharge of the electrode or cell as a whole. Such phenomenological methodologies inevitably make use of approximate fitting parameters like the maximum degree of discharge. This does yield valuable information on the discharge process, but using it is impossible to study the effect of the porous active-material behavior, the distribution of discharge parameters inside the porous particle, the blocking, shrinking and critical radii, and thus on the overall discharge process. Therefore, the introduction of new and more advanced applications of batteries has led to an increasing need for simple mathematical models that are able to simulate complicated discharge process.

The models presented here are simple and useful to gain a physical understanding of the dynamic characteristics occurring in the porous negative electrode of the lead-acid battery. The developed models are based on the principles of chemical reaction engineering [25]. This considers the fluid-particle electrochemical reaction in a separate grain of lead and offers a simple method for calculating the characteristics of discharge of an electrode plate. Moreover, while deriving the shrinking core model, the effects of several parameters including the double-layer effect are taken into account. In general, non-Faradic phenomena play a very important role in the time-dependent electrode potential and which predominates initially. To validate the model's capability to accurately simulate these effects, model predictions are compared to experimental discharge data gathered by using Bitrode's model LCN2-250-12 [26]. This is a computer-controlled laboratory test system for measuring discharge capabilities of automotive and industrial batteries. LCN circuits have an important place in research and quality-assurance laboratories testing batteries to rigorous standards, and enabling the development of new materials.

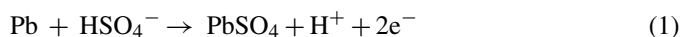
Three different model systems are described based on the degree of complexity. In all these systems, the unreacted-core shrinking boundary is defined, assuming a precipitation–dissolution mechanism. The three possible fields on which the models are based are: (i) concentration-gradient domain; (ii) potential-gradient domain; (iii) coupled concentration and potential gradients. The discharge process is governed by a partial differential equation that describes the way that the potential or concentration of electrochemically active species changes in the vicinity of the particle as a function of both time and distance. During the process of computation, possible analytical solutions are used to enable exact solutions. Unfortunately, analytical solutions are not available for all the cases of interest. In that situation, numerical techniques must be used to solve the model equations. The new separation of variables method [27] is used for solving the model equation that governs the concentration-gradient domain. In the other cases, the model comprised a system of time-dependent reaction-diffusion equations, coupled through the nonlinear reaction terms with mixed Dirichlet and Neumann boundary conditions. To compute the solutions, the numerical method of lines (MOL) is used. It is a straightforward and effective approach for solving parabolic

PDEs [28]. This method is particularly helpful when analyzing the behavior of a system with respect to time.

The purpose of these models is to give a qualitative analysis rather than an exact, detailed description. Although the model is applied to the lead-acid battery, the modeling approach appears to be generally applicable to model constant-current discharging curve of other batteries, such as lithium-ion or metal-hydride [29]. The rest of the article is organized as follows: the model equations for different domains are derived in Section 2; in Section 3 the numerical results are plotted with comparison to the experimental data, thus providing a detailed insight into the electrode operation, and finally Section 4 gives a summary of the results.

## 2. Description of mathematical models

The negative electrode is made up of densely packed lead particles with a rough surface whose sphericity,  $\phi$  (defined as the surface–volume ratio for a sphere of diameter  $D_p$  divided by surface–volume ratio for the particle whose nominal size is  $D_p$ ) may approximately be 0.8; because of this, the lead-negative active material has a network structure on close packing. There are large numbers of active sites present on the lead particles of which most nucleate and grow as a result of the reaction of  $\text{Pb}^{2+}$  ions with  $\text{HSO}_4^-$  ions from the solution. The rate of crystal growth depends on the over-saturation, temperature, and electrolyte concentration. The lead crystals are interconnected forming a highly porous reactive structure, which is transformed fully into  $\text{PbSO}_4$  during discharge. Another part of the crystals forms the so-called skeleton structure with small surfaces, which is not discharged but ensures an electronic conductive path within the electrode. The ratio between both structures determines the negative active-material discharge efficiency. The discharge process of the negative electrode begins when the bisulphate ion diffuses into an active lead surface; then at the interface the lead reacts electrochemically with bisulphate ions as follows:



The discharge process is complete when the effective diffusion length inside the particle is beyond the diffusion coefficient of bisulphate ions.

The shrinking core model can be introduced to investigate this situation, wherein it is hypothetically assumed that the reactive structure forms the shrinking Pb cores and the product  $\text{PbSO}_4$  forms the ash layer. The reaction occurs first at the outer skin of the particle, then the zone of reaction moves into the solid, leaving behind a completely converted reactive structure and an unreacted skeleton structure. Thus, at any time there exists an unreacted skeleton structure, which ensures the electronic conductive pathways in the electrode. This model is depicted in Fig. 1 which consists of the following regions and boundary: a shrinking region of unreacted lead core with the formation of poorly soluble low-conducting product region and the shrinking boundary at the interface.

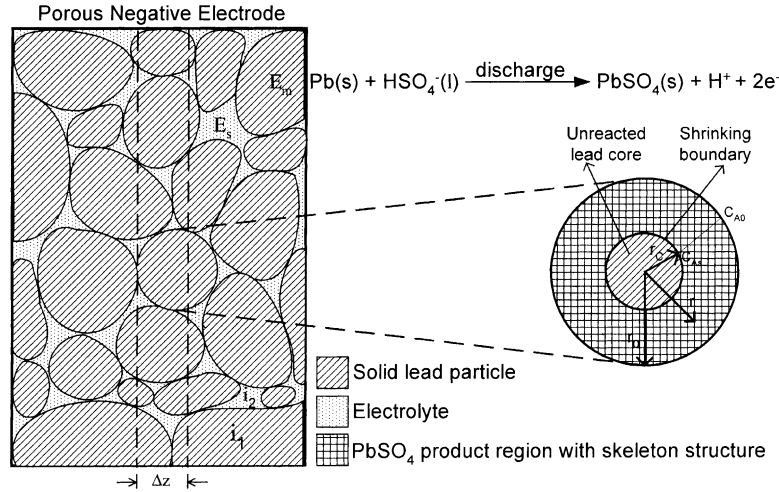


Fig. 1. Schematic drawing of negative electrode of a lead-acid battery cell according to the shrinking core concept.

The following simplifying assumptions are made regarding kinetics and transport mechanisms: (i) the acid solution is taken to be a concentrated binary electrolyte which completely dissociates into  $\text{HSO}_4^-$  and  $\text{H}^+$  ions, (ii) discharge of Pb to  $\text{PbSO}_4$  is a dissolution–precipitation process, (iii) constant current is applied at the surface of the particle, (iv) separability of total current density into Faradic and non-Faradic current densities, (v) the lead-negative active material is packed with spherical lead particles of unit sphericity, (vi) double-layer capacitance, transfer coefficients and transference number are constants. This process is modeled in one-dimensional spherical coordinate based on the different approximations.

### 2.1. The concentration-gradient domain

Consider a single spherical particle of the porous electrode as shown in Fig. 1. As the particle is discharged, the core of the active-material shrinks. Based on the assumptions, the concentration distribution of the bisulphate ions in the product region is given by:

$$\frac{\partial \varepsilon C_A}{\partial t} = \frac{\varepsilon D_{\text{eff}}}{r^2} \frac{\partial}{\partial r} \left( r^2 \frac{\partial C_A}{\partial r} \right) \quad (2)$$

where  $\varepsilon$  is the porosity of the spherical lead particle,  $D_{\text{eff}}$  is the effective diffusivity of the binary electrolyte and it is given by Bruggeman's relation [30] as  $D_{\text{eff}} = \varepsilon^{0.5} D$ . At the shrinking core boundary ( $r_c$ ), the concentration can be expressed in terms of applied current flux:

$$D_{\text{eff}} \frac{\partial C_A}{\partial r} = \frac{-i}{nF} \quad \text{at } r = r_c \quad (3)$$

It is assumed that the concentration at the outer surface is equal to the initial acid concentration, hence:

$$C_A = C_{A0} \quad \text{at } r = r_0 \quad (4)$$

Initial condition is given as:

$$C_A = 0 \quad \text{at } t = 0 \quad (5)$$

In Eq. (3),  $i$  is the applied current density at the surface; it can be conveniently expressed in terms of applied current per gram as follows:

$$i = I \rho \frac{(4/3)\pi r_0^3}{4\pi r_0^2} = \frac{I \rho r_0}{3} \quad (6)$$

Here,  $I$  is the applied current density per gram of the active material and  $\rho$  is the density of the particle. Eq. (6) is used to modify Eq. (3) as:

$$D_{\text{eff}} \frac{\partial C_A}{\partial r} = \frac{-I \rho r_0}{3nF} \quad (7)$$

The electrochemical reaction rate at the moving interface is equal to the mass flux at the interface, thus the motion of interface is given by:

$$\frac{dr_c}{dt} = - \frac{D_{\text{eff}}}{\rho} \frac{\partial C_A}{\partial r} \Big|_{r=r_c} \quad (8)$$

The dimensionless variables are defined as follows:

$$x = \frac{r}{r_0}; \quad x_c = \frac{r_c}{r_0}; \quad \tau = \frac{D_{\text{eff}} t}{r_0^2}; \quad C = \frac{C_A}{C_{A0}} \quad (9)$$

$$\rho^* = \frac{C_{A0}}{\rho}; \quad I^* = \frac{I \rho r_0^2}{3nF D_{\text{eff}} C_{A0}}$$

Substituting these dimensionless variables into Eq. (2) gives:

$$\frac{1}{x^2} \frac{\partial}{\partial x} \left( x^2 \frac{\partial C}{\partial x} \right) = \frac{\partial C}{\partial \tau} \quad (10)$$

The initial and boundary conditions becomes:

$$C = 0; \quad \tau = 0$$

$$C = 1; \quad x = 1 \quad (11)$$

$$\frac{\partial C}{\partial x} = -I^*; \quad x = x_c$$

and also

$$\frac{dx_c}{d\tau} = -\rho^* \left. \frac{\partial C}{\partial x} \right|_{x=x_c} \quad (12)$$

Analytical expressions for the above boundary value problem can be obtained by using a new separation of variables method [27]. Let us introduce the following variable transformation:

$$C(x, \tau) = u(x, \tau) + w(x) \quad (13)$$

Here  $w(x)$  satisfies the inhomogeneous boundary conditions:

$$x = 1; \quad w = 1 \quad (14)$$

and

$$x = x_c; \quad \frac{dw}{dx} = -I^* \quad (15)$$

The variable  $u(x, \tau)$  satisfies the homogeneous boundary conditions and also the initial condition as follows:

$$x = 1; \quad u = 0 \quad (16)$$

$$x = x_c; \quad \frac{\partial u}{\partial x} = 0 \quad (17)$$

$$u = -w; \quad \tau = 0 \quad (18)$$

The transformation given by Eq. (13) changes Eq. (10) to:

$$\frac{1}{x^2} \frac{\partial}{\partial x} \left( x^2 \frac{\partial u}{\partial x} \right) + \frac{1}{x^2} \frac{\partial}{\partial x} \left( x^2 \frac{\partial w}{\partial x} \right) = \frac{\partial u}{\partial \tau} \quad (19)$$

Separating the variables, we get:

$$\frac{d}{dx} \left( x^2 \frac{dw}{dx} \right) = 0 \quad (20)$$

and

$$\frac{1}{x^2} \frac{\partial}{\partial x} \left( x^2 \frac{\partial u}{\partial x} \right) = \frac{\partial u}{\partial \tau} \quad (21)$$

Now  $w(x)$  can be solved easily with the boundary conditions to give:

$$w(x) = 1 + x_c^2 I^* \left( \frac{1}{x} - 1 \right) \quad (22)$$

Hence, the solution is given by:

$$C(x, \tau) = 1 + x_c^2 I^* \left( \frac{1}{x} - 1 \right) + u(x, \tau) \quad (23)$$

Now  $u(x, \tau)$  is obtained by solving Eq. (21) with the homogeneous boundary conditions Eqs. (16) and (17) to give:

$$u(x, \tau) = -\frac{1}{x} \sum_{n=1}^{\infty} A_n \sin[\lambda_n(1-x)] \exp(-\lambda_n^2 \tau) \quad (24)$$

where  $A_n$  ( $n = 1, 2, \dots$ ) are constants.  $A_n$  is obtained by imposing the initial condition Eq. (18) and  $\lambda_n$  is eigenvalue given by:

$$\tan[\lambda_n(1-x_c)] + \lambda_n x_c = 0 \quad (25)$$

Thus, the final solution is expressed as:

$$C(x, \tau) = 1 + x_c^2 I^* \left( \frac{1}{x} - 1 \right) - \frac{1}{x} \sum_{n=1}^{\infty} A_n \sin[\lambda_n(1-x)] \exp(-\lambda_n^2 \tau) \quad (26)$$

where

$$A_n = \frac{2(x_c I^* - 1)}{\lambda_n} \quad (27)$$

and  $x_c$  is obtained by integrating Eq. (12) using explicit stepping.

Eq. (26) is the analytical solution for the dimensionless concentration as a function of dimensionless distance and discharge time. Knowing the value of  $x_c$ , the profiles of concentration inside the particle can be obtained. Using Eq. (26), the distribution of surface concentration can also be evaluated by setting  $x = x_c$ . In any electrochemical systems, the electrochemical behavior is completely determined by the concentration at the surface [31].

### 2.2. The potential-gradient domain

Consider the porous electrode models developed by Rangarajan [32] and Semenenko [17] with regard to potential-gradient domain. To easily handle this physical reality, assume that at any point in space in the electrode we have only the solid reactant, product and electrolyte. Then on an inert free basis the volume fractions of the three add up to one. A current balance on an element of volume  $A dz$ , across the porous electrode is:

$$[I\epsilon A]_z^{z+\Delta z} = - \int_z^{z+\Delta z} ja\epsilon_s A dz \quad (28)$$

where  $j$  is the interfacial current density, i.e. the current transferred from the matrix phase to solution phase,  $I$  the applied current density,  $a$  the surface area per unit volume of the porous electrode particle,  $\epsilon_s$  the volume fraction of solid reactant and  $\epsilon$  the void fraction. Application of the mean value theorems to Eq. (28) gives:

$$\epsilon \frac{\partial I}{\partial z} = -a\epsilon_s j \quad (29)$$

Conservation of charge requires that the total current density is the sum of the matrix ( $i_1$ ) and solution ( $i_2$ ) phase current densities:

$$i_1 + i_2 = I \quad (30)$$

Combining Eqs. (29) and (30), the interfacial current density is related to the gradient of current densities as:

$$-\epsilon \frac{\partial i_1}{\partial z} = \epsilon \frac{\partial i_2}{\partial z} = a\epsilon_s j \quad (31)$$

The interfacial current density is expressed as the sum of the double-layer charging current density and the Faradic current density:

$$j = i_{nF} + i_F = C_{dl} \frac{\partial(E_m - E_s)}{\partial t} + i_F \quad (32)$$

$C_{dl}$  is the double-layer capacitance. The kinetic behavior of a lead electrode in the lead-acid battery during discharge has been presented by Ekdunge and Simonsson [11] and the Faradic current density,  $i_F$ , is written as follows:

$$i_F = i_0 \left( 1 - \frac{Q}{Q_{max}} \right) \frac{1 - \exp[(\alpha_a + \alpha_c)(F/RT)(E_m - E_s)]}{(ai_0/i_{lim}) - \exp[\alpha_c(F/RT)(E_m - E_s)]} \quad (33)$$

Here the limiting current density  $i_{lim}$  affects significantly the polarization curves and is determined from the dissolution rate of lead, the diffusion rate of lead ions and the precipitation rate of lead sulfate crystals ( $i_{lim} = -2.5 \times 10^4 \text{ A m}^{-3}$ ). The electrochemically active area 'a' can be related to the state of discharge as:

$$a = a_{max} \left( \frac{Q}{Q_{max}} \right)^S \quad \text{and} \quad \frac{dQ}{dt} = \frac{1}{2F} \left( \frac{di_2}{dz} \right) = \frac{1}{2F} j \quad (34)$$

where  $a_{max}$  denotes the active surface area of the electrode at the fully charged state,  $Q$  the charge density in the electrode,  $Q_{max}$  the theoretical maximum capacity, and  $S$  the shape factor which relates the state of discharge with the surface area.

With no concentration gradients, the matrix-phase current density,  $i_1$ , and solution-phase current density,  $i_2$ , are given by Ohm's law [33]:

$$i_1 = -\sigma_{eff} \frac{\partial E_m}{\partial z} \quad (35)$$

$$i_2 = -\kappa_{eff} \frac{\partial E_s}{\partial z} \quad (36)$$

where  $\sigma_{eff}$  and  $\kappa_{eff}$  are the effective matrix-phase and solution-phase conductivities, respectively. Bruggeman's relation [30] is used to determine the effective parameters of the porous electrode from the bulk values:

$$\sigma_{eff} = (1 - \varepsilon)^{1.5} \sigma \quad (37)$$

$$\kappa_{eff} = \varepsilon^{1.5} \kappa \quad (38)$$

Changes in porosity can be equated to volume differences between solid products and reactants resulting from the local

$$x = \frac{r}{r_0}; \quad x_c = \frac{r_c}{r_0}; \quad \eta^* = \frac{F}{RT} \eta; \quad \tau = \frac{t}{a\varepsilon_s C_{dl} [(1/\sigma_{eff}) + (1/\kappa_{eff})] r_0^2} \quad (46)$$

$$I^* = \frac{F}{RT} \frac{r_0}{\kappa_{eff}} I; \quad J = \frac{F}{RT} a\varepsilon_s r_0^2 \left[ \frac{1}{\sigma_{eff}} + \frac{1}{\kappa_{eff}} \right] i_0; \quad I_0^* = \frac{i_0}{i_{lim}}; \quad q = \frac{Q}{Q_{max}}$$

transfer current, and may be expressed by:

$$\frac{\partial \varepsilon}{\partial t} = \frac{1}{2F} \left[ \frac{M_{Pb}}{\rho_{Pb}} - \frac{M_{PbSO_4}}{\rho_{PbSO_4}} \right] j \quad (39)$$

Differentiating Eq. (35) and substituting in Eq. (31) gives the governing equation for the solid-phase potential:

$$\sigma_{eff} \frac{\partial^2 E_m}{\partial z^2} = a\varepsilon_s j \quad (40)$$

Similarly, the governing equation for the solution-phase potential is given by combining Eq. (31) and differentiation of Eq. (36):

$$\kappa_{eff} \frac{\partial^2 E_s}{\partial z^2} = a\varepsilon_s j \quad (41)$$

The overpotential is given by  $\eta = E_m - E_s$  when the open-circuit potential is set equal to zero. For a constant value for the open-circuit potential ( $E \neq 0$ ) the quantity  $(E_m - E_s)$  in Eq. (33), and consequently in the following expressions should be replaced with  $\eta = E_m - E_s - E$ . Based on this definition of the overpotential, the governing equation for potential distribution inside the spherical particle can be expressed as second-order non-linear partial differential equation using Eqs. (32), (40) and (41):

$$\frac{1}{r^2} \frac{\partial}{\partial r} \left( r^2 \frac{\partial \eta}{\partial r} \right) = \left( \frac{1}{\sigma_{eff}} + \frac{1}{\kappa_{eff}} \right) \left[ a\varepsilon_s C_{dl} \frac{\partial \eta}{\partial t} + a\varepsilon_s i_0 \left( 1 - \frac{Q}{Q_{max}} \right) \times \frac{1 - \exp[(\alpha_a + \alpha_c)(F/RT)\eta]}{(ai_0/i_{lim}) - \exp[\alpha_c(F/RT)\eta]} \right] \quad (42)$$

The initial condition is:

$$\eta = 0 \quad \text{at} \quad t = 0$$

The boundary conditions are:

$$\eta = \eta_0 \quad \text{at} \quad r = r_0 \quad (43)$$

$$-\frac{\partial \eta}{\partial r} = \frac{I}{\kappa_{eff}} \quad \text{at} \quad r = r_c \quad (44)$$

$\eta_0$  is the overpotential at the surface of the particle. Since the rate of electrochemical reaction at the interface is proportional to the applied current, using Faraday's law the motion of the interface is given by the current flux at the interface:

$$\frac{dr_c}{dt} = -\frac{\kappa_{eff}}{nF\rho} \frac{\partial \eta}{\partial r} \Big|_{r=r_c} \quad (45)$$

Let us introduce the following dimensionless variables:

then the equations can be written in dimensionless form as:

$$\frac{1}{r^2} \frac{\partial}{\partial r} \left( r^2 \frac{\partial \eta^*}{\partial r} \right) = \frac{\partial \eta^*}{\partial \tau} + J(1 - q) \frac{1 - e^{(\alpha_a + \alpha_c)\eta^*}}{I_0^* - e^{\alpha_c \eta^*}} \quad (47)$$

with the initial and boundary conditions:

$$\eta^* = 0; \quad \tau = 0 \tag{48a}$$

$$\eta^* = \eta_0^*; \quad x = 1 \tag{48b}$$

$$-\frac{\partial \eta^*}{\partial x} = I^*; \quad x = x_c \tag{48c}$$

and interface position as:

$$\frac{dx_c}{d\tau} = -\left. \frac{\partial \eta^*}{\partial x} \right|_{x=x_c} \tag{49}$$

Since the reaction kinetics is represented by nonlinear source terms, the search for analytical solutions is not possible. The Eqs. (47)–(49) have to be solved numerically. Nevertheless, analytical solutions are the best if available or can be obtained. For this reason and to force the parameters in a correct direction that gives the best results with the certainty that they correspond with physical reality. The analytical solution is achieved by replacing the nonlinear source terms by means of linearized kinetics. Then this expression is used in aiding the numerical computation of above nonlinear PDE using the MOL.

Suppose that the overall discharge current density is not very high, and suffice it to restrict the calculation to linear members of the exponent expansion in Butler–Volmer kinetics within a Taylor series. Then the Faradic current density ( $i_F$ ) is given by the linearized Butler–Volmer kinetics [34]. Based on this simplification, Eq. (47) becomes:

$$\frac{\partial^2 \eta^*}{\partial x^2} + \frac{2}{x} \frac{\partial \eta^*}{\partial x} = \frac{\partial \eta^*}{\partial \tau} + J\eta^* \tag{50}$$

with the same boundary conditions Eq. (48). With the intention of converting the PDE Eq. (50) to a solvable form, the following variable transformation is applied.

$$\bar{\eta}^* = \eta^* \exp(J\tau) \tag{51}$$

Then the problem becomes:

$$\frac{1}{x^2} \frac{\partial}{\partial x} \left( x^2 \frac{\partial \bar{\eta}^*}{\partial x} \right) = \frac{\partial \bar{\eta}^*}{\partial \tau} \tag{52}$$

with the boundary conditions:

$$\begin{aligned} \bar{\eta}^* &= 0; \quad \tau = 0 \\ \bar{\eta}^* &= \bar{\eta}_0^*; \quad x = 1 \\ -\frac{\partial \bar{\eta}^*}{\partial x} &= I^* \exp(J\tau); \quad x = x_c \end{aligned} \tag{53}$$

Now applying the same procedure as followed in Section 2.1, the final analytical solution for the above Eqs. (52) and (53) after transforming back to  $\eta^*$  is given by:

$$\begin{aligned} \eta^*(x, \tau) &= \eta_0^* + x_c^2 I^* \left( \frac{1}{x} - 1 \right) \\ &\quad - \frac{1}{x} \sum_{n=1}^{\infty} A_n \sin[\lambda_n(1-x)] \exp(-\lambda_n^2 \tau) \end{aligned} \tag{54}$$

where,

$$A_n = \frac{2(x_c I^* - \eta_0^*)}{\lambda_n} \tag{55}$$

and  $\lambda_n$  is obtained by using the Eq. (25).

The numerical procedure for solving the actual nonlinear problem Eq. (47), using the boundary conditions Eq. (48) and linearized analytical solution Eq. (54) are given in Section 3.

### 2.3. Coupled concentration and potential gradients

By taking into account the charge-transfer reaction, charging and discharging of the electric double-layer at the interface, changes in porosity, and specific surface area and charge conservation reaction, the material balance for the bisulfate ion Eq. (2) can be rewritten as:

$$\begin{aligned} \frac{\partial \varepsilon C_A}{\partial t} &= \varepsilon D_{\text{eff}} \frac{1}{r^2} \frac{\partial}{\partial r} \left( r^2 \frac{\partial C_A}{\partial r} \right) \\ &\quad + a(1 - 2t_+^0) j_n + \frac{a C_{\text{dl}}(1 - 2t_+^0)}{nF} \frac{\partial \eta}{\partial t} \end{aligned} \tag{56}$$

where  $t_+^0$  is the transference number of bisulfate ions in the solution and  $j_n$  the pore wall flux of ions across the interface between the electrolyte and the active material. For a dissolution–precipitation mechanism, it is assumed that the electrode reactions in the negative electrode consists of three steps, i.e., dissolution of lead sulfate, diffusion of lead ions to the active sites, and precipitation of lead [11], by including the dependence of the electrolyte concentration the Faradic current is written as follows:

$$\begin{aligned} i_F &= j_n F = i_0 \left( 1 - \frac{Q}{Q_{\text{max}}} \right) \left( \frac{C_{As}}{C_{A0}} \right)^\gamma \\ &\quad \times \frac{1 - \exp[(\alpha_a + \alpha_c)(F/RT)\eta]}{ai_0/i_{\text{lim}} - \exp[\alpha_c(F/RT)\eta]} \end{aligned} \tag{57}$$

where  $\gamma$  is the exponent for the concentration dependence and  $C_s$  the surface concentration, the concentration at the interface or shrinking boundary ( $\gamma=0.01$ ). The variation in the porosity and specific surface area are given by Eqs. (34) and (39). Due to the existence of concentration gradient, the solution-phase potential is governed by modified Ohm’s law as:

$$i_2 = -\kappa_{\text{eff}} \frac{\partial E_s}{\partial x} + \frac{2RT\kappa_{\text{eff}}}{FC_{Ai}} (1 - 2t_+^0) \frac{\partial C_A}{\partial x} \tag{58}$$

$C_{Ai}$  is the concentration of bisulfate ions in the solution phase at open-circuit conditions. Incorporating the modified Ohm’s law, the potential distribution Eq. (47) can be rewritten as follows:

$$\begin{aligned} \frac{1}{r^2} \frac{\partial}{\partial r} \left( r^2 \frac{\partial \eta}{\partial r} \right) &= \left( \frac{1}{\sigma_{\text{eff}}} + \frac{1}{\kappa_{\text{eff}}} \right) \left[ a\varepsilon_s C_{\text{dl}} \frac{\partial \eta}{\partial t} + a\varepsilon_s i_F \right] \\ &\quad - \frac{2RT\kappa_{\text{eff}}(1 - 2t_+^0)}{FC_{Ai}} \frac{\partial C_A}{\partial r} \end{aligned} \tag{59}$$

For both the dependent variables (concentration and overpotential), initial and boundary conditions are the same as discussed in

Table 1  
Dimensionless variables [35]

Dimensionless parameters	Definition
$v^2$	$\frac{a i_0 F n}{RT} \left( \frac{1}{\sigma_{\text{eff}}} + \frac{1}{\kappa_{\text{eff}}} \right) r_0^2$
$B_1$	$\left( \frac{F^2 \varepsilon C_{A1}}{RT(1-2r_+^0)} \right) \frac{1}{a C_{dl}}$
$B_2$	$\left( \frac{F^2 \varepsilon C_{A1}}{RT(1-2r_+^0)} \right) D_{\text{eff}} \left( \frac{1}{\sigma_{\text{eff}}} + \frac{1}{\kappa_{\text{eff}}} \right)$

the previous sections. Introducing the following dimensionless dependent variables:

$$C = \frac{C_A}{C_{A0}} \quad \text{and} \quad \eta^* = \frac{F}{RT} \eta \quad (60)$$

and the dimensionless independent variables:

$$x = \frac{r}{r_0} \quad \text{and} \quad \tau = \frac{t}{a \varepsilon_s C_{dl} \left[ (1/\sigma_{\text{eff}}) + (1/\kappa_{\text{eff}}) \right] r_0^2} \quad (61)$$

Eqs. (56) and (59) can be written in dimensionless form as follows:

$$\frac{1}{x^2} \frac{\partial}{\partial x} \left( x^2 \frac{\partial C}{\partial x} \right) = \frac{B_1}{B_2} \frac{\partial C}{\partial \tau} - \frac{v^2}{B_2} C(1-q) \frac{1 - e^{(\alpha_a + \alpha_c)\eta^*}}{I_0^* - e^{\alpha_c \eta^*}} - \frac{1}{B_2} \frac{\partial \eta^*}{\partial \tau} \quad (62)$$

$$\frac{1}{x^2} \frac{\partial}{\partial x} \left( x^2 \frac{\partial \eta^*}{\partial x} \right) = \frac{\partial \eta^*}{\partial \tau} + v^2 C(1-q) \frac{1 - e^{(\alpha_a + \alpha_c)\eta^*}}{I_0^* - e^{\alpha_c \eta^*}} - 2(1-2r_+^0) \frac{\partial^2 C}{\partial x^2} \quad (63)$$

where  $v_2$ ,  $B_1$  and  $B_2$  are dimensionless groups defined in Table 1. The boundary conditions in dimensionless form then become:

$$\text{at } x = 1 \quad \eta^* = \eta_0^* \quad (64)$$

$$C = 1$$

$$\text{at } x = x_c \quad -\frac{\partial \eta^*}{\partial x} = I^* \quad (65)$$

$$-\frac{\partial C}{\partial x} = I^*$$

and the initial condition is:

$$\text{at } \tau = 0 \quad \eta^* = 0 \quad (66)$$

$$C = 0$$

Eqs. (62) and (63) have to be solved simultaneously subject to Eqs. (64)–(66).

### 3. Results and discussions

Very often, analytical solutions involve integrals, eigenvalues, etc., which must be evaluated numerically. Hence the solution procedures are programmed in a symbolic language: Maple [36]. This software allows many numerical techniques, symbolic

Table 2

Model parameters used for simulation of discharge process of a lead particle inside the lead-acid battery

Parameters	Values	Reference
Initial acid concentration, $C_{A0}$	0.00504 mol cm <sup>-3</sup>	[18]
Diffusion coefficient of H <sub>2</sub> SO <sub>4</sub> , $D$	2.59E-5 cm <sup>2</sup> s <sup>-1</sup>	[18]
Capacity, $Q$	257 mAh g <sup>-1</sup>	[11]
Exchange current density, $i_0$	1.41 mA g <sup>-1</sup>	[12]
Charge-transfer coefficient of Pb electrode	$\alpha_a = 1.55$ , $\alpha_c = 0.45$	[12]
Thermodynamic potential of lead, $E_0$	-0.35 V	[19]
Cut-off potential, $E_c$	-0.20 V	[19]
Void fraction, $\varepsilon$	0.6	[11]
Volume fraction of solid reactant, $\varepsilon_s$	0.4	[11]
Shape factor, $S$	0.95	[7]
Radius of the particle, $r_0$	3 μm	[11]
Discharge rate	257 mAh g <sup>-1</sup> ( $I^* = 1.4$ )	[11]
Solution-phase conductivity, $\kappa$	2300 S cm <sup>-1</sup>	[11]
Solid-phase conductivity, $\sigma$	4.8E4 S cm <sup>-1</sup>	[11]

and also graphical mathematical computations. The computational procedures are executed using the base value given in Table 2.

#### 3.1. Effect of applied current density on shrinking interface

The values of the first five eigenvalues are obtained by setting  $x_c$  equal to a value (say 0.99) and solving Eq. (25). Then this computation is repeated by giving a decrement of 0.01 till  $x_c$  reaches zero. Given the first five eigenvalues as a function of dimensionless interface position, Eq. (12) is integrated numerically by explicit stepping. This step can be implemented using the following explicit relation and specifying a value for  $\Delta\tau$ .

$$x_c(\tau + \Delta\tau) = x_c(\tau) + \Delta\tau \left( \rho^* \frac{\partial C}{\partial x} \Big|_{x=x_c} \right) \quad (67)$$

Here  $x_c = 1$  at  $\tau = 0$ , the concentration gradient in Eq. (67) is obtained from Eq. (26) for any specified value of dimensionless applied current density. The same procedure is followed in potential-gradient domain to obtain the shrinking interface position as a function of discharge time. In this case, Eq. (49) is integrated with the initial condition and the gradient is obtained from Eq. (54). But the eigenvalues remain the same for both the cases. For a particular value of  $\tau$ ,  $C$  and  $\eta$  are solved by using Maple's fsolve command.

Fig. 2 shows the dimensionless interface position as a function of dimensionless time at various levels of applied current density ( $I^*$ ). It represents the results obtained from the analytical expressions derived for both concentration as well as potential gradients domain. For an applied current density ( $I^* = 0.5$ ), at very low times, the interface position is almost near the surface of the particle, i.e., close to  $r_0$ . As the time increases, the core radius shrinks. However, at higher applied current density ( $I^* > 1.0$ ) the core radius shrinks very fast right from the beginning of discharge process. This is true because at high discharge rates, the particle discharges faster; thus, concentration or potential gradient values are high. The slope decreases

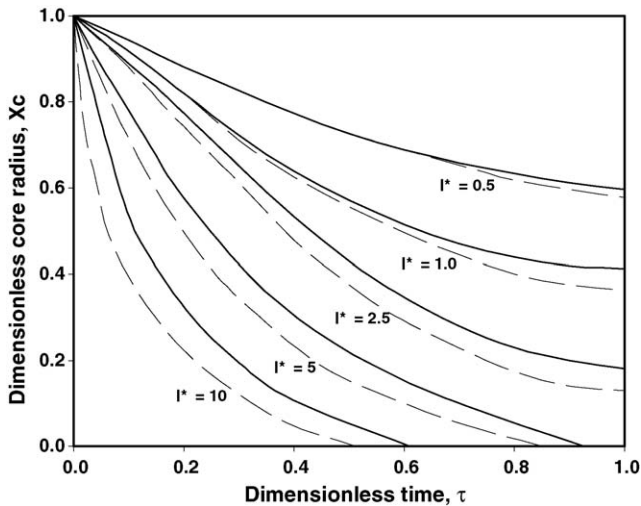


Fig. 2. Dimensionless shrinking core radius as a function of dimensionless discharge time for two different models, — Eq. (49), --- Eq. (12).

gradually. Also it can be observed that the shrinking core position is much less when compared with discharge at low rates. As can be seen in the plot, the concentration gradients domain model under predicts the time for the unreacted core to shrink, but for low values of the parameter both the models nearly coincide. This is not surprising because the former model is only a measure of mass-transport behavior and acid availability within a porous lead particle, which has been reasonably well modeled.

### 3.2. The concentration and potential distributions

The analytical solution given by Eq. (26) depends on  $x_c$  and time,  $\tau$ . Consequently, to obtain  $C(x, \tau)$  for given parameter values, first step is to know the value of  $x_c$  as a function of discharge time. This can be obtained from the previous plot between the dimensionless interface position and discharge time for any value of  $I^*$ . Then Eq. (26) can be easily solved to get the profiles of dimensionless concentration distribution as a function of dimensionless discharge time. Maple’s fsolve command can execute this computation readily.

But to evaluate the profiles of dimensionless potential distribution, the nonlinear PDE Eq. (47) has to be solved using the boundary and initial conditions Eq. (48) along with Eq. (49). For this purpose the numerical MOL is used. It is a general technique for solving nonlinear PDEs by typically using finite difference relationships for the spatial derivatives and ordinary differential equations for the time derivative. The method proceeds in two separate steps: (i) spatial derivatives are first replaced with finite difference approximations, (ii) the resulting system of usually stiff, semi-discrete (discrete in space and continuous in time) ordinary differential equations is integrated in time. Thus the  $x$ -axis is discretized into  $N$  equal intervals, so that there are  $n = N + 1$  internal node points. The step-size in  $x$ -axis is then given by,

$$\Delta x = \frac{1 - x_c}{N} \tag{68}$$

Thus, for 10 equally spaced intervals we have  $n = 11$  internal node points. Now it is required to seek expressions for the dependent variable at all the 11 node points ( $\eta_1, \eta_2, \eta_3, \dots, \eta_{11}$ ). The boundary condition at  $x = x_c$  (Eq. (48c)) can be rewritten using a first-order finite difference as:

$$-\frac{\eta_2^* - \eta_1^*}{\Delta x} = I^* \tag{69}$$

This can be solved for  $\eta_1$  to yield:

$$\eta_1^* = \eta_2^* + \Delta x I^* \tag{70}$$

and the boundary condition at  $x = 1$  (Eq. (48b)) gives,

$$\eta_{11}^* = \eta_0^* \tag{71}$$

The particle is initially held at zero potential. This gives the initial condition that all the interior node potentials are known at time  $\tau = 0$ .

$$\eta_n^* = 0 \quad \text{for } n = 2, \dots, 10 \text{ at } \tau = 0 \tag{72}$$

The dependent variables at the interior node points ( $\eta_2, \eta_3, \eta_4, \dots, \eta_{10}$ ) satisfy the governing Eq. (47) with the second derivative in  $x$  expressed in three-point central difference form accurate to the order  $(\Delta x)^2$  are

$$\frac{d\eta_n^*}{d\tau} = \frac{\eta_{n+1}^* - 2\eta_n^* + \eta_{n-1}^*}{(\Delta x)^2} + \frac{2(\eta_{n+1}^* - \eta_n^*)}{n(\Delta x)^2} - J(1 - q) \frac{1 - e^{(\alpha_a + \alpha_c)\eta^*}}{I_0^* - e^{\alpha_c \eta^*}} \quad \text{for } n = 2, \dots, 10 \tag{73}$$

Thus using the MOL, the nonlinear system has been reduced to an ODE system in time. The problem then requires the solution of Eqs. (70), (71) and (73) which results in nine simultaneous nonlinear ordinary differential equations and two explicit algebraic equations for the 11 unknown potentials at the various nodes. To solve this stiff system, one can use the dsolve solver in Maple with automatic step-size and order control with stiff equal to true option that is suitable to capture the initial transient layer both accurately and efficiently. The finite difference semi-discretization involves integrals of the nonlinear reaction terms on the right hand side of Eq. (73). Usually, these integrals would require a numerical approximation. Instead, we take advantage of the special form of the dsolve command by setting stiff equal to true. When this method is specified, a consistency check is also performed to verify that the method matches with the stiff value. The technique is both accurate and simple in solving the problem Eqs. (70)–(73) effectively.

Figs. 3 and 4 show the converged concentration and potential distributions, respectively, as a function of different discharge time for an applied current density,  $I^* = 2.5$ . The plot of the electrolyte-concentration profile at different stage of discharge time (Fig. 3) provides us with information on the availability of the acid for the electrode reaction. The profiles indicate whether acid depletion is limiting the capacity of the cell. For the present case bisulphate ions depletion at the shrinking core is definitely a limiting factor. The bisulphate ions depletion at

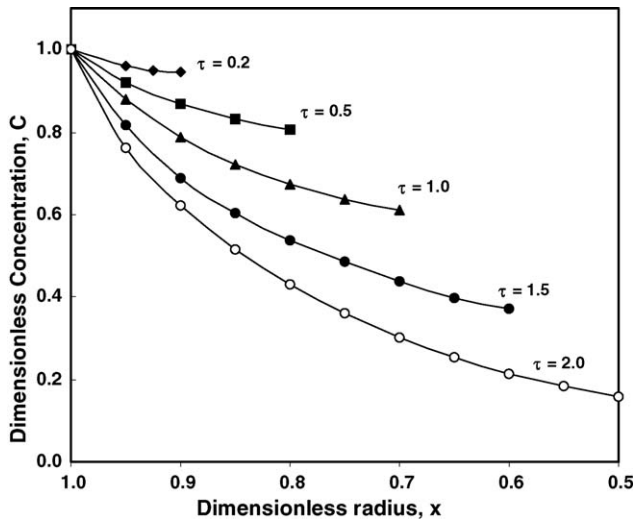


Fig. 3. Dimensionless concentration profiles for the electrochemical reaction as a function of radial distance and discharge time due to applying a dimensionless current density,  $I^* = 2.5$ .

the shrinking interface is very difficult to measure experimentally during rapid discharge. But an interpretation of this process is achieved from the solution of developed model equations. It is apparent from this figure that the bisulphate ions concentration near the surface of the particle is close to unity at very low times. As time increases, the bisulphate ions concentration depletes very fast and the core shrinks leading to the end of discharge. The effect of maintaining the concentration constant at this point in effect assumes a well-stirred acid recirculation of electrolyte at a practical temperature. In a single electrode, this is made possible by placing the electrode in a large volume of acid and maintaining a well-stirred solution. In a typical cell stack, only density differences, volume changes, and gassing promote stirring and contact with remote acid volumes. Therefore, in a normal cell stack, without forced electrolyte flow, the

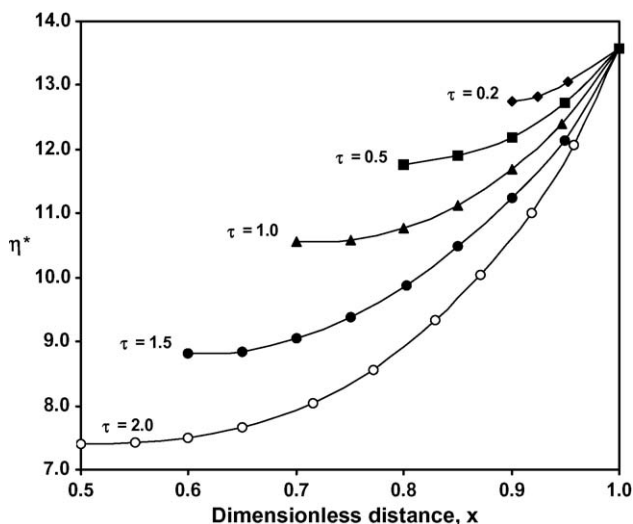


Fig. 4. Dimensionless potential distributions along the particle distance as a result of applying a dimensionless current density,  $I^* = 2.5$ .

performance of the cell will be greatly affected by the volume of solution contained between the densely packed lead particles.

The degree of polarization across the thickness of an electrode particle is the  $\eta^*$  profiles. For the present case, Fig. 4 indicates that the polarization of the negative particle is relatively unchanged during the initial stages of discharge. Towards the end of discharge, the degree of polarization becomes more uniform. The acid concentration may play a role in the difference between the high- and low-polarization profiles. As bisulphate ions depletion begins to become significant, the potential drops. But it is maintained to some extent in the particle due to high diffusivity. With increasing discharge time the potential decreases on approaching the particle center. Thus, in usual conditions, the particles are presumably small, the discharge occurs at a uniform distribution of potential inside them, the reaction rate is the same across the particle bulk and it is much simpler to model the discharge process.

### 3.3. Discharge curves

The model equations in concentration-gradient domain can be used to obtain the discharge curves by expressing the kinetics at the surface as:

$$I = I_0 \left( 1 - \frac{Q}{Q_{\max}} \right) \left( \frac{C_s}{C_{A0}} \right)^\gamma \frac{1 - \exp[(\alpha_a + \alpha_c)(F/RT)\eta]}{a i_0 / i_{\lim} - \exp[\alpha_c(F/RT)\eta]} \quad (74)$$

where  $C_s$  is the dimensionless surface concentration and  $I_0$  the exchange current per unit mass. The potential at the surface is given by:

$$E(V) = E_0 + \eta \quad (75)$$

The above two equations are used to predict the discharge curves and the procedure consists of first setting  $I$  and the parameter values, followed by solving the governing equations to obtain Eq. (26), and hence  $C_s(\tau)$  by setting  $x = x_c$ . Next, once values have been set for  $I_0$ ,  $E_0$ ,  $\alpha$ , and  $\tau$ , Eq. (74) can be used to solve for  $\eta(\tau)$ , which upon substitution into Eq. (75) yields  $E(\tau)$ . For a particular time  $\tau$  and  $C_s$ ,  $\eta$  is solved using Maple's solve command. Once the overpotential  $\eta$  is found, Eq. (75) is used to find the potential. This procedure is repeated until a cut-off potential of  $E_c = -0.2$  V is reached. For the case of the model equations in potential-gradient domain,  $\eta(\tau)$  can be obtained directly by using the Eqs. (70)–(73). The state of discharge (SOD) is defined here as:

$$\text{SOD} = \frac{I(\text{current applied, A g}^{-1}) \times t(\text{s}) \times 100}{Q(\text{capacity, Ah g}^{-1}) \times 3600} \quad (76)$$

In the case of the coupled concentration and potential gradients domain, the model equations Eqs. (62)–(66) are solved using the same numerical MOL as demonstrated in Section 3.2 for Eqs. (47) and (48). Here additionally one more set of equations in concentration domain are to be solved. The final semi-discretized form of the governing equations in concentration domain is

expressed as:

$$C_1 = C_2 + \Delta x I^*$$

$$\begin{aligned} & \frac{-1}{B_2} \frac{d\eta_n^*}{d\tau} + \frac{B_1}{B_2} \frac{dC_n}{d\tau} \\ &= \frac{C_{n+1} - 2C_n + C_{n-1}}{(\Delta x)^2} + \frac{2(\eta_{n+1}^* - \eta_n^*)}{n(\Delta x)^2} + \frac{v^2}{B_2} C_n(1 - q) \\ & \times \frac{1 - e^{(\alpha_a + \alpha_c)\eta_n^*}}{I_0^* - e^{\alpha_c \eta_n^*}} \quad \text{for } n = 2, \dots, 10, \quad C_{11} = 1 \quad (77) \end{aligned}$$

with the initial condition  $C_n = 0$  for  $n = 2, \dots, 10$  at  $\tau = 0$  and in potential domain it is given by (by assuming Ohm's law for solution-phase potential):

$$\eta_1^* = \eta_2^* + \Delta x I^*$$

$$\begin{aligned} \frac{d\eta_n^*}{d\tau} &= \frac{\eta_{n+1}^* - 2\eta_n^* + \eta_{n-1}^*}{(\Delta x)^2} + \frac{2(\eta_{n+1}^* - \eta_n^*)}{n(\Delta x)^2} - v^2 C_n(1 - q) \\ & \times \frac{1 - e^{(\alpha_a + \alpha_c)\eta_n^*}}{I_0^* - e^{\alpha_c \eta_n^*}} \quad \text{for } n = 2, \dots, 10, \quad \eta_{11}^* = \eta_0^* \quad (78) \end{aligned}$$

and also  $\eta_n^* = 0$  for  $n = 2, \dots, 10$  at  $\tau = 0$ .

The above two set of equations are strongly coupled nonlinear ODEs. All these equations can be integrated simultaneously using a convenient ODE solver package such as Maple's dsolve command. On the other hand, the surface concentration distribution obtained from the analytical solution Eq. (26) can be substituted directly in Eq. (77) to get the  $\eta(\tau)$ . This procedure requires only one set of semi-discretized equations to be solved. Fig. 5 shows the dimensionless surface concentration distribution in the active particle as a function of applied current density. As expected, the surface concentrations depleted faster for higher rates. Also, we observe that the discharge time, which is the time taken for surface concentration to reach approximately zero, is highly dependent on the dimensionless current density. When these data are effectively utilized in place of Eq.

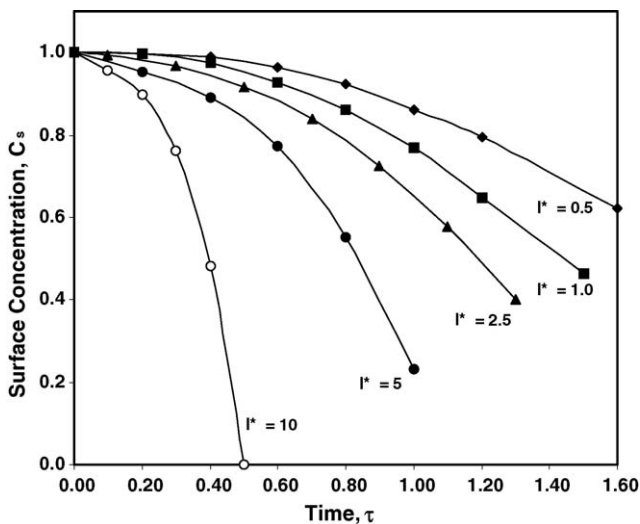


Fig. 5. Surface concentration variation during the course of discharge reaction.

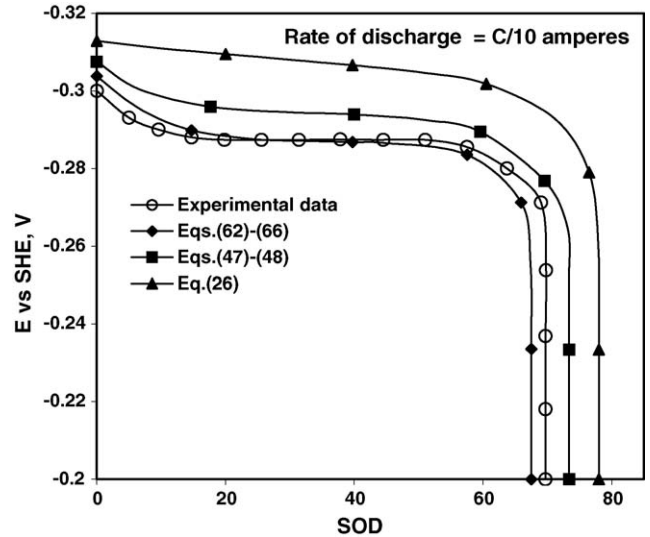


Fig. 6. Comparison of theoretically predicted and experimental discharge curves. SOD, state of discharge.

(77), one can easily obtain the  $\eta(\tau)$ , and hence the SOD with minimal computational effort.

Three numbers of 2 V/64 Ah<sub>10</sub> Planté type lead-acid cells with flat negative plates were discharged in series using the Bitrode's model LCN2-250-12 at a current of 6.4 A equivalent to 10 h rate of discharge. The negative plate potential was monitored using a cadmium reference electrode and the values are converted to SHE reference, taking the  $E^0$  value of the Cd/Cd<sup>2+</sup> as  $-0.40$  V. The data are acquired with a computer-controlled data acquisition system. Although the collected data are rather extensive, comparisons of the measured data with the three different models are shown in Fig. 6. The agreement between experiment and theory appears reasonably good. In particular the agreement is superior for the third model comparing with the first two models; here we see more of a difference between the experimental and predicted curves due to much simplification in model equations. Careful inspection of the experimental data might suggest a slight deviation than would be theoretically predicted. At a given discharge rate, the theoretical lies above the experimental in the initial portion of discharge and crosses over the experimental curve near the end of discharge. The initial drop in the experimental discharge curve is generally attributed to super saturation of PbSO<sub>4</sub> in sulfuric acid solutions. This effect is not included in the model. A partial explanation of the higher predicted voltage lies in the uncertainty in the anodic charge-transfer coefficient of the Pb electrode, as well as in the uncertainty in the value of exchange current densities of the electrodes. Considering the possible magnitude of the errors, there appears to be reasonably good agreement between experiment and theory.

Fig. 7a shows the discharge curves at different discharge rates for both the cases of with and without double-layer charging effect. During discharge, the shrinking interface where the electrochemical reaction takes place moves from the outer surface towards the center of the electrode. Therefore, the length of the current path in the electrolyte-filled pores increases with

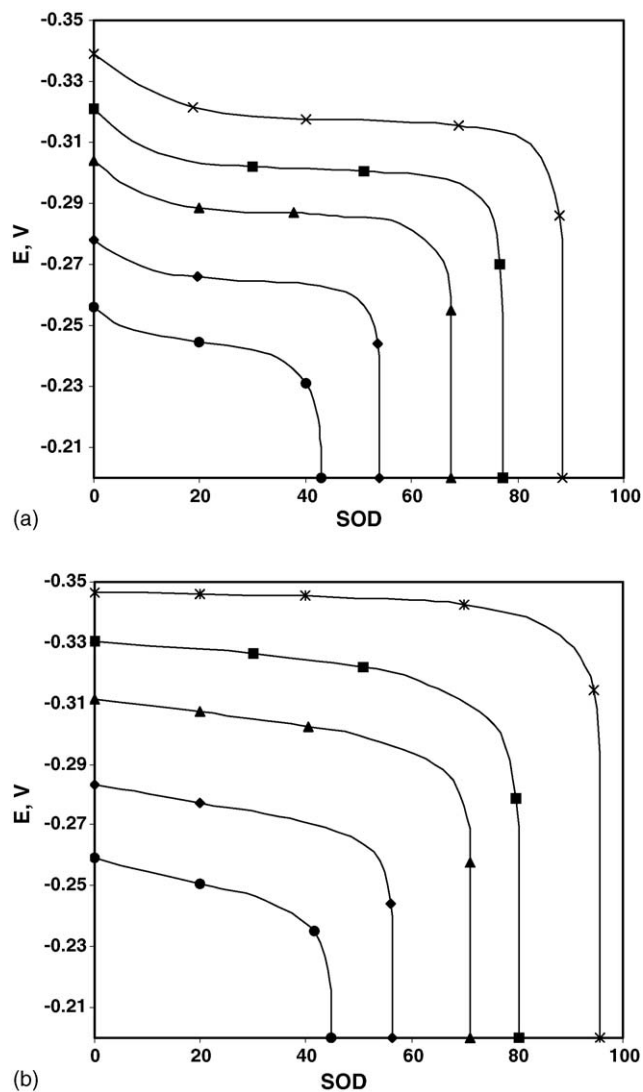


Fig. 7. (a) The discharge curves obtained at different discharge rates. (b) The corresponding results with  $C_{dl}=0$ . (Discharge curve with marker  $\times$  represents  $C/10$  rate, marker  $\blacksquare$  represents  $C/2$  rate, marker  $\blacktriangle$  represents  $C$  rate, marker  $\blacklozenge$  represents  $2C$  and marker  $\bullet$  represent  $3C$  rate.)

depth-of-discharge. For higher discharge rates the particle discharges fast, and  $E$  reach  $-0.2$  V in lesser time. It is due to the fact that the effective conductivity of the electrolyte in the distance between the particle surface and the reaction zone does not offer any additional resistance. This plot also shows the results when ignoring the double-layer capacitance. The study of electrical double-layer is important because the charge distribution in a given system influences the electron transfer, and thus the course of electrochemical reaction. The non-Faradic contribution is very high during the beginning of discharge process due to the charging of double layer and equilibrium concentration. Fig. 7b shows that double-layer charging has an impact over the process till the discharge termination.

It is observed from the above investigation that the predicted SOD of the particle with shrinking core concept is closer to the experimental data at high discharge rates, i.e., rate more than  $C/10$ . But at lower rates these are much less than the experimental

data. Thus, for predicting the utilization factor accurately, especially at high discharge rates the shrinking core model should be used.

#### 4. Conclusions

A theoretical model for the porous lead electrode is proposed on the basis of the unreacted-core shrinking model used for the fluid-particle reactions. From this investigation it is obvious that the shrinking core cannot be ignored in porous lead particles discharging at the negative plate of lead-acid batteries. As expected, the models state that for higher discharge rates the particle discharges faster ( $E$  reach  $-0.2$  V in less time). At the end of discharge a layer of lead sulphate crystals blocks the electrode surface in the outer layers of the electrode. The current can then neither be transferred across this insulated surface nor reach remaining active material in the inner parts of the electrode because of acid depletion. This situation is furthermore accelerated by the decreasing porosity and electrochemically active area. In this account an analytical expression is achieved, and the calculations show that quite remarkable concentration gradients are possible in such electrode. It is also observed that the time needed to reach the steady state is much longer than what was expected. When the coupled potential and concentration gradients are considered, this discharge time is beyond the supposed discharge time.

The concentration gradients domain model with an analytical solution can only be an average model for the negative plate. However, it has the merit to give a better understanding of the fundamental problems than with a pure computer simulation. In the next two models, the number of parameters to be estimated is large. Thus the numerical MOL is adopted to solve these model equations. The partial derivatives are discretized in the radial direction, and the resulting ODE system is integrated in time using a convenient solver packages. The parameters are forced hopefully in a better direction using a simplified analytical solution.

Using these models, different valuable results can be obtained. Such knowledge would allow suggesting modifications in a system to obtain desired changes. Also this model could help in advanced development of a system by providing a quick means of examining the effects of various parameters on the system's performance. The study has good scope in optimizing the concentration and potential profiles. The optimization process will also assist in extending the lifetime of a lead-acid battery.

#### Acknowledgements

Research fellowship awarded to B. Vijayasekaran, jointly by the Council of Scientific & Industrial Research, New Delhi, India, and Central Electrochemical Research Institute, Karaikudi, India, is thankfully acknowledged. Also acknowledges Dr. P.G. Balakrishnan, Scientist, Lead-Acid Battery Section, CECRI, for his helpful discussions. Special thanks are due to Prof. A.K. Shukla, Director, CECRI for his encouragement.

## References

- [1] C.M. Shepherd, *J. Electrochem. Soc.* 112 (1965) 657–664.
- [2] D. Simonsson, *J. Appl. Electrochem.* 3 (1973) 261–270.
- [3] D. Pavlov, *J. Electroanal. Chem.* 72 (1976) 319–327.
- [4] K. Mica, I. Rousar, *Electrochim. Acta.* 21 (1976) 599–603.
- [5] P. Horvath, P. Jedlovsky, M. Benedek, *J. Power Sources* 8 (1982) 41–54.
- [6] A.D. Turner, P.T. Moseley, *J. Power Sources* 9 (1983) 19–40.
- [7] G. Sunu, in: R.E. White (Ed.), *Electrochemical Cell Design*, Plenum Press, New York, 1984, pp. 357–376.
- [8] S. Atlung, B. Fastrup, *J. Power Sources* 13 (1984) 39–54.
- [9] H. Gu, T.V. Nguyen, R.E. White, *J. Electrochem. Soc.* 134 (1987) 2953–2960.
- [10] P. Ekdunge, K.V. Rybalka, D. Simonsson, *Electrochim. Acta* 32 (1987) 659–667.
- [11] P. Ekdunge, D. Simonsson, *J. Appl. Electrochem.* 19 (1989), Part I: pp. 127–135, Part II: pp. 136–141.
- [12] T.V. Nguyen, R.E. White, H. Gu, *J. Electrochem. Soc.* 137 (1990) 2998–3010.
- [13] R.M. LaFollette, D.N. Bennion, *J. Electrochem. Soc.* 137 (1990) 3701–3707.
- [14] P. Ekdunge, *J. Power Sources* 46 (1993) 251–262.
- [15] D. Baert, A. Vervaet, *Electrochim. Acta* 44 (1999) 3491–3504.
- [16] H.A. Catherino, J.F. Burgel, A. Rusek, F. Feres, *J. Power Sources* 80 (1999) 17–20.
- [17] M.G. Semenenko, *Russian J. Electrochem.* 40 (2004) 98–101.
- [18] T.V. Nguyen, R.E. White, *Electrochim. Acta* 38 (1993) 935–945.
- [19] D.M. Bernardi, M.K. Carpenter, *J. Electrochem. Soc.* 142 (1995) 2631–2641.
- [20] J. Newman, W. Tiedemann, *J. Electrochem. Soc.* 144 (1997) 3081–3091.
- [21] R.L. Cantrell, D.B. Edwards, P.S. Gill, *J. Power Sources* 73 (1998) 204–215.
- [22] S.C. Kim, W.H. Hong, *J. Power Sources* 89 (2000) 93–101.
- [23] R.J. Ball, R. Evans, R. Stevens, *J. Power Sources* 103 (2002) 213–222.
- [24] M. Thele, S. Buller, D.U. Sauer, R.W. De Doncker, E. Karden, *J. Power Sources* 144 (2005) 461–466.
- [25] O. Levenspiel, *Chemical Reaction Engineering*, third ed., Wiley, NJ, 1999, pp. 570–577.
- [26] <http://www.bitrode.com>.
- [27] V.R. Subramanian, R.E. White, *J. Power Sources* 96 (2001) 385–395.
- [28] M.E. Davis, *Numerical Methods and Modeling for Chemical Engineers*, Wiley, New York, 1984, pp. 127–175.
- [29] V.R. Subramanian, H.J. Ploehn, R.E. White, *J. Electrochem. Soc.* 147 (2000) 2868–2873.
- [30] P. De Vodts, R.E. White, *J. Electrochem. Soc.* 144 (1997) 1343–1353.
- [31] B. Vijayasekaran, C. Ahmed Basha, *Electrochim. Acta* 51 (2005) 200–207.
- [32] S.K. Rangarajan, *J. Electroanal. Chem.* 22 (1969) 89–104.
- [33] J. Newman, *Electrochemical Systems*, second ed., Prentice Hall, Englewood Cliffs, NJ, 1991.
- [34] K. Scott, *Electrochemical Reaction Engineering*, Academic Press, London, 1991.
- [35] S. Devan, V.R. Subramanian, R.E. White, *J. Electrochem. Soc.* 151 (2004) A905–A913.
- [36] <http://www.maplesoft.com>.